Integration of functional brain information into stereotactic irradiation treatment planning using magnetoencephalography and MR-axonography

Hidefumi Aoyama M.D, PhD,[1] Kyousuke Kamada M.D, PhD,[2] Hiroki Shirato M.D, PhD,[1] Fumiya Takeuchi PhD,[3] Shinya Kuriki PhD,[3] Yoshinobu Iwasaki M.D, PhD,[2] Kazuo Miyasaka M.D, PhD.[1]

1. Department of Radiology, Hokkaido University Graduate School of Medicine, Sapporo, Japan.

2. Department of Neurosurgery, Hokkaido University Graduate School of Medicine, Sapporo, Japan.

3. Research Institute of Applied Electricity, Hokkaido University, Sapporo, Japan.

Address for correspondence:
Hidefumi Aoyama, M.D., PhD.
Department of Radiology, Hokkaido University Graduate School of Medicine, North-15 West-7, Kita-ku, Sapporo, Japan, 060-8638
Tel: 81-11-716-1161; Fax: 81-11-706-7876;
e-mail: hao@radi.med.hokudai.ac.jp

Presented in part at the American Society for Therapeutic Radiology and Oncology (ASTRO) Annual Meeting, New Orleans, Louisiana, October 2002.

Running title: Functional imaging for STI planning

Pages: 20; Tables: 1; Figures: 5

ABSTRACT

Purpose: To minimize the risk of neurological deficit following stereotactic irradiation, functional brain information was integrated into treatment planning.

Materials and Methods: Twenty-one magnetoencephalography and 6 magnetic resonance axonographic images were made in 20 patients in order to evaluate the sensorimotor cortex (n=15 patients, including the corticospinal tract in 6), the visual cortex (n=4) and the Wernicke's area (n=2). One radiation oncologist was asked to formulate a treatment plan without the functional images at first, and then to modify the plan after seeing them. The pre- and post-modification values were compared for the volume of the functional area receiving 15 Gy or more (V_{15}), and the volume of the PTV receiving more than 80% of the prescribed dose (V_{80}-PTV).

Results: Fifteen out of 21 plans (71%) were modified after seeing the functional images. After modification, V_{15} was significantly reduced compared to the values of pre-modification in those 15 sets of plans ($p=0.03$), whereas there was no significant difference in V_{80}-PTV ($p=0.99$). During follow-up, a radiation-induced necrosis at the corticospinal tract caused minor motor deficit in one patient for whom MR-axonography was not available in the treatment planning. No other radiation-induced functional deficit was observed in the other patients.

Conclusions: Integration of MEG and MR-axonography in treatment planning has the potential to reduce the risk of radiation-induced functional dysfunction without deterioration of the dose distribution in the target volume.

Key words: Radiosurgery, Magnetoencephalography, Axon, Function, Arteriovenous malformation

Introduction

One of the advantages of stereotactic irradiation (STI) over surgical resection in the treatment of brain diseases is that STI is an easier and safer method of accessing areas deep in the brain, as well as those located in the vicinity of the functional brain cortex. Permanent radiation injury, known as radiation necrosis, is not a common consequence of STI. However, once necrosis occurs in certain areas of the brain responsible for the motor function, visual function, or comprehension or production of speech, it results in permanent neurologic deficits [1-4]. The development of radiation necrosis is related to the dose of radiation received. Considering that neuronal fibers are serial in structure, the severity of neurologic deficit is expected to be related to factors such as the maximum radiation dose administered to functional brain areas, as well as the volume of the area exposed to more than the threshold dose of radiation [5,6]. Although the threshold dose of radiation required to develop radiation necrosis has not been fully investigated, some clinical and experimental data have indicated that the threshold single dose lies within the range of 10-15 Gy [3,4,7].

Recently, imaging modalities that enable the identification of functional brain areas have emerged as clinically significant [8-18]. Magnetoencephalography (MEG) is used

to detect the magnetic field associated with intracranial neuronal electric activity itself. In practice, it has been used to identify the sensorimotor, visual, and Wernicke's speech cortices [8,10,11,12]. Magnetic resonance (MR) axonography or anisotropic diffusion weighted MR imaging (ADWI) is a method that visualizes the axonal pathway in the brain. ADWI applies three-orthogonal diffusion gradient pulses and can clearly demonstrate neuronal fibers perpendicular to a diffusion gradient as a hyperintense area. Theoretically, all the subcortical tracts that run in the cranial-caudal direction become hyperintense in the anterior-posterior (AP) diffusion gradient; however, previous reports on ADWI have suggested that the hyperintense areas might consist mainly of corticospinal tract [16, 17, 18].

Integration of the three-dimensional configuration of functional brain areas into conformal radiation treatment planning using MEG and ADWI may minimize the risk of developing symptomatic adverse effects due to radiation necrosis at the functional brain area. In this study, we evaluated the potential contribution of integrating functional information into radiation treatment planning by dose-volume statistics to reduce the risk of symptomatic radiation necrosis. Preliminary clinical outcomes are also reported.

Materials and Methods

Twenty patients (8 female and 12 male; median age, 45 years; range, 11-82 years) with intracranial diseases located near or within the functional cortex or the corticospinal tract were included in this study. The patients' characteristics are listed in Table 1. Five patients had brain metastases and 15 had arteriovenous malformations (AVMs). One of the patients with metastases received STI for two lesions, and thus 21 lesions were included. Functional brain areas were identified by MEG in all 21 areas of the 20 patients. Six recent cases in which the lesions were close to the corticospinal tract pathway were evaluated by using ADWI as well. The follow-up duration ranged from 3 to 35 months (mean, 12 months).

The MEG studies were performed in a magnetically shielded room with a 204-channel wholehead biomagnetometer (VectorView; 4D-Neuroimage, San Diego, CA). The spatial resolution of MEG to detect the location of functional cortex is considered to be less than 5 mm [8-12] For the identification of the sensorimotor cortex in 15 patients, a somatosensory mapping protocol was used in which the median and tibial nerves contralateral to the side of the lesion were stimulated at the wrist and ankles, respectively, with 0.2 msec constant-current pulses. For the primary visual cortex mapping in 4 patients (**Figure 1**), the visually evoked field was measured by standard

pattern shift stimulation. The Wernicke's area was identified by a simple object-naming task in 2 right-handed patients (**Figure 2**). In the evaluation of corticospinal tract using ADWI, hyperintense areas with an intensity 1.6 times higher than that of normal white matter in the anterior-posterior diffusion gradient were considered as part of the corticospinal tract (**Figure 3**). Anatomical, ADW imaging experiments were performed during the MRI investigation using a 1.5 T whole-body MR scanner with echo-planner capabilities and a standard whole-head transmit-receiver coil (Magnetom Vision; Siemens AG, Erlangen, Germany). Four sessions of multislice single-shot spin-echo echo-planar ADW imaging (TE, 87 msec.; 128 x 128 matrix; 19 slices) were performed with a b value of 1000 seconds/mm^2. After the raw data of each ADW imaging session were 2-dimensionally reconstructed, all four sessions of ADW imaging were averaged. The diffusion gradients were applied sequentially in three orthogonal directions to generate three sets of transverse ADW images to visualize the tract orientation. Because the CST was theoretically expected to be the most hyperintense area in the anterior-posterior diffusion gradient, we took as the CST those hyperintense areas having intensity 1.6 times higher than the normal white matter. Anatomical 3D MR imaging data of each patient's head was obtained, resulting in 128 sequential, 1.8-mm-thick axial slices with a resolution of 256 x 256 pixels in FOV of 300 mm. Both

data from the MEG dipole and the ADWI were integrated into an anatomical 3D-MR image herein referred to as a function-integrated MRI.

The MRI can be registered with the with the CT image using a CT-MR fusion system (EV pro, Hitachi Medico Co., Ltd., Tokyo), as described in detail previously [19]. The anatomical CT for radiation planning was conducted by conventional CT machine (Sfida, SCT-7000TX/TH; Shimazu, Kyoto) with slice thickness of 3 or 5 mm with matrix size of 256 x 256 with FOV of 280 mm. In brief, registration of the CT and MR images can be conducted based on 4 or more anatomical landmarks (e.g., the bilateral cochlea, the top of the basilar artery, the anterior commissure, etc.). After the registration, the contoured region-of-interest (ROI), such as the tumor or the organs-at-risk on the MR image, is automatically superimposed on the relevant CT image. In the same manner, after the registration of the function-integrated MRI with the CT image, the functional area was contoured on MRI and then superimposed on the relevant CT images. The CT images with the contours of tumors, anatomical organs-at-risk, and functional area (i.e., the function-integrated CT images) can be transferred to a 3D-RTP system (FOCUS; CMS Co., Ltd., St. Louis, MO) and used for dose calculation with inhomogeneity correction. STI was performed with a 6 mega-voltage linac-based stereotactic system (CLINAC 2300 C/D, Varian, CA) using treatment parameters

transferred via Ethernet. The setup accuracy of the system was estimated to be ± 1 mm.

In this study, treatment plans were first created using conventional MRI/CT fusion images without functional data by one radiation oncologist who was blinded to the information regarding functional brain areas. After the radiation oncologist had completed the planning, the treatment plans were modified using function-integrated CT images. We evaluated the influence of the integration of functional information into the planning by comparing dose-volume statistics between the two consecutive plans for the same patient. The final treatment plans formulated using the function-integrated CT were chosen for the actual treatment.

Radiation was delivered radiosurgically in a single session to 5 lesions ranging in isocentric doses from 20 Gy to 25 Gy (median, 20 Gy). Ten other lesions were treated with hypofractionated STI using 20 to 35 Gy (median, 35 Gy) at the isocenter in 4 fractions. The PTV was covered with an 80-90% isodose surface. In order to simplify the evaluation, each schedule of hypofractionated dose was converted into a single fraction schedule using a linear-quadratic model with an alpha/beta ratio of 2 for normal tissue. The maximum dose (D_{max}) to the functional area and the volume of the functional area receiving 10 Gy or more (V_{10}) and 15 Gy or more (V_{15}) were used to evaluate the effect on the functional area. The dose that 95% of the planning target

volume received (D_{95}-PTV) and the amount of planning target volume receiving 80% or more of the prescribed dose (V_{80}-PTV) were used to evaluate the effect on the target volume. Student's *t*-test was used for the comparison. Values of $p<0.05$ were considered to indicate statistical significance.

Results

Dose-Volume Statistics

The functional cortex was successfully identified in all 21 regions by using MEG. The corticospinal tract pathway was also well identified using ADWI in all six patients examined. Fifteen (71%) out of 21 plans were judged to have been modified using the function-integrated CT images, and only 6 (29%) remained unchanged.

In the 15 lesions for which the plan was modified, the D_{max}, V_{10}, and V_{15} of the functional area after the modification were consistently reduced compared to the plan without functional information. The mean D_{max}, V_{10}, and V_{15} before modification were 15.5 Gy, 2.1 cc, and 1.8 cc and were reduced to 13 Gy, 0.9 cc, and 0.5 cc after modification. The reduction was not significant for D_{max} ($p=0.24$) or V_{10} ($p=0.12$), but it was significant for V_{15} ($p=0.03$) (**Figure 4**). In all 21 lesions, the average D_{max} value was 13.7 Gy (standard deviation (SD): 6.53 Gy) before the modification and 12.0 Gy (SD: 6.4)

after the modification (p=0.41). In total, V_{10} was 1.8 cc (SD: 2.3) before the modification and 0.9 cc (SD: 1.3) after the modification (p=0.17); V_{15} was 1.3 cc (SD: 1.3) before modification and 0.4 cc (SD: 0.7) after modification (p=0.04).

In the 15 sets of plans that were modified after seeing the functional information, there was no significant dose reduction in PTV. D_{95}-PTV was 18.5 Gy (SD: 4.5) before modification and 17.8 Gy (SD: 4.0) after modification (p=0.66); V_{80}-PTV was 4.02 cc (SD: 2.15) before modification and 4.02 cc (SD: 2.15) after modification (p=0.99) (**Figure 4**). In all 21 sets of plans, no reduction was seen in PTV after modification, as expected. The mean D_{95}-PTV of the 21 plans was 18.4 Gy (SD: 4.2Gy) and 17.9 Gy (SD 3.7Gy) before and after the modification (p=0.66); V_{80}-PTV was 5.131 cc (SD: 5.27) before and 5.132 cc (SD: 5.27) after the modification (p=0.99).

Functional outcome

Adverse events after STI occurred in 4 patients. One patient with AVM suffered from intracranial bleeding and died 3 months after STI (case 14). Other adverse events included an increased signal on T2-weighted MRI in 2 patients (case 10 and case 13) and radiation necrosis in 1 patient (case 4). The former two patients did not complain of any neurologic symptoms. The patient with radiation necrosis complained of a minor motor deficit, which showed limitation of movement of the left ankle. This

patient had an AVM at the corpus callosum and received MEG but not ADWI before radiosurgery. ADMI was performed when he complained of a motor deficit. It showed radiation injury to the corticospinal pathway (**Figure 5**).

Discussion

Over the past decade, an increasing body of evidence has indicated that larger doses of radiation lead to better cures of AVM and brain metastases after STI [1,2,20,21]. In order to obtain a cure or local control of disease, coverage of the disease by at least 15 Gy has generally been considered necessary for AVM [1] and 18-20 Gy or more was recommended for brain metastases [20,21]. However, such treatment schedules are consistently accompanied by a 3-7% risk of developing radiation necrosis [1,2,3,4,20,21]. The degree of neurological deficit is associated with the location and the size of the radiation necrosis [3,4]. Therefore, if functional areas are not involved in the high dose area, patients would be symptom-free even if they had radiation necrosis in a silent area. Precise integration of functional images is expected not only to reduce radiation injury but also to increase the cure rate of the AVM and tumors by allowing delivery of a sufficient dose without fear of adverse reactions.

Apart from MEG, functional MRI (fMRI) and positron emission tomography (PET)

is reported to be useful functional imaging modalities and fMRI is used for radiotherapy-treatment planning [14,15]. MEG provides the direct measure of neuronal electric activity. In comparison with MEG, fMRI and PET provide the three-dimensional representation of functional activity in the brain in terms of metabolic and hemodynamic variables, and the relationship between those variables and neuronal activity has not yet well defined. Although fMRI can localize the functional cortex, its efficacy and validity for AVM are reported to be low [13]. The major issue is that functional brain mapping by fMRI is based on hemodynamic changes, and thus it might be affected if autoregulation of the blood flow is lost in brain tissue near AVM. In contract, MEG detects the magnetic field associated with intracranial neuronal electric activity itself, and thus is not influenced by a high blood flow shunt [13]. Therefore, it is reasonable to use MEG in patients with AVM [13]. ADMI that visualizes the axonal pathway in the brain has emerged as a potentially useful tool to supplement these images [16,17,18]. Kamiryo *et al.* recently developed a technique combining MEG data and angiography as a tool to provide simultaneous viewing of both modalities in three dimensions. They reported that this technique may reduce the risks associated with embolization treatment [13]. A group in New Jersey used fMRI for radiosurgical planning and succeeded at reducing the maximum dose to the functional

area in three patients in the treatment planning with an average dose reduction of 32% [14, 15].

In the present series, MEG was used in 21 regions in 20 cases in order to localize the sensorimotor cortex, the visual cortex, and the Wernicke's area. We also used AWDI in addition to MEG in the 6 more recent cases. DVH analysis revealed that the area of functional brain tissue receiving 15 Gy was significantly reduced when plans were modified after the functional information was provided, whereas coverage of PTV was not significantly deteriorated. One patient with AVM at the corpus callosum who did not receive ADWI experienced a minor motor deficit, indicating that functional imaging of the relevant cortex is not sufficient to reduce symptomatic complications. Injury to the corticospinal tract was suggested to be reduced by the use of ADWI.

In conclusion, we here developed a method of integrating information about the functional cortex and corticospinal tract into STI planning. Although further investigation will be necessary in order to fully understand the contribution of functional imaging study, the results presented here indicate that the integration of functional brain information could potentially reduce the risk of developing neurologic functional disturbance after undergoing STI.

References

1. Touboul E, Al Halabi A, Buffat L, *et al*. Single-Fraction Stereotactic Radiotherapy: A Dose-Response Analysis of Arteriovenous Malformation Obliteration. *Int J Radiat Oncol Biol Phys* 1998; 41: 855-861.

2. Aoyama H, Shirato H, Nishioka T, *et al*. Treatment outcome of single or hypofractionated stereotactic irradiation (STI) using a linear accelerator for intracranial arteriovenous malformation. *Radiother Oncol* 2001; 59: 323-328.

3. Flickinger JC, Kondziolka D, Lunsford LD, *et al*. Development of a model to predict permanent symptomatic postradiosurgery. *Int J Radiat Oncol Biol Phys* 2000; 46: 1143-1148.

4. Voges J, Treuer H, Sturm V, *et al*. Risk analysis of linear radiosurgery. *Int J Radiat Oncol Biol Phys* 1996; 36: 1055-1063.

5. Kallman P, Agren A, and Brahme A. Tumour and normal tissue responses to fractionated non-uniform dose delivery. *Int J Radiat Biol* 1992; 62: 249-262.

6. Niemierko A, and Goitein M. Modeling of normal tissue response to radiation: the critical volume model. *Int J Radiat Oncol Biol Phys* 1992; 25: 135-145.

7. Fike JR, Cann CE, Turowski K, *et al*. Radiation dose response of normal brain. *Int J Radiat Oncol Biol Phys* 1998; 14: 63-70.

8. Kamada K, Takeuchi F, Kuriki S, *et al*. Functional neurosurgical stimulation with brain surface magnetic resonance images and magnetoencephalography. *Neurosurg* 1993; 33: 269-273.

9. Schulder M, Maldjian JA, Liu WC *et al*. Functional image-guided surgery of intracranial tumors located in or near the sensorimotor cortex. *J Neurosurg* 1998; 89: 412-418.

10. Ganslandt O, Fahlbusch R, Nimsky C, *et al*. Functional neuronavigation with magnetoencephalography: outcome in 50 patients with lesions around the motor cortex. *J Neurosurg* 1999; 91: 73-79.

11. Kamada K, Kober H, Saguer M, *et al*. Response to silent *Kanji* reading of the native Japanese and German in task subtraction magnetoencephalography. *Cognitive Brain Research* 1998; 7: 89-98.

12. Alberstone CD, Skirboll SL, Benzel EC, *et al*. Magnetic source imaging and brain surgery: presurgical and intraoperative planning in 26 patients. *J Neurosurg* 2000; 92: 79-90.

13. Kamiryo T, Cappell J, Kronberg E, *et al*. Interactive use of cerebral angiography and magnetoencephalography in arteriovenous malformations: technical note. *Neurosurg* 2002; 50: 903-911.

14. Liu WC, Schulder M, Narra V, *et al*. Functional magnetic resonance imaging aided radiation treatment planning. *Med Phys* 2000; 27: 1563-1572.

15. Shulder M, Vega J, Narra V, *et al*. Functional magnetic resonance imaging and radiosurgical planning. *Stereotact Funct Neurosurg* 1999; 73: 38-44.

16. Nakada T, Nakayama N, Fujii Y, *et al*. Clinical application of three-dimensional anisotropy contrast magnetic resonance axonography. *J Neurosurg* 1999; 90: 791-795.

17. Karibe H, Shimizu H, Tominaga T, *et al*. Diffusion-weighted magnetic resonance imaging in the early evaluation of corticospinal tract injury to predict functional motor outcome in patients with deep intracerebral hemorrhage. *J Neurosurg* 2000; 95: 58-63.

18. Holodny AI, Ollenschleger MD, Liu WC, *et al*. Identification of the corticospinal tracts achieved using blood-oxygen-level-dependent and diffusion functional MR imaging in patients with brain tumors. *AJNR* 2001; 22: 83-88.

19. Aoyama H, Shirato H, Nishioka T, *et al*. Magnetic resonance imaging (MRI) system for three-dimensional conformal radiotherapy (3D-CRT) and its impact on gross tumor volume (GTV) delineation of central nervous system (CNS) tumors. *Int J Radiat Oncol Biol Phys* 2001; 50: 821-827.

20. Shiau CY, Sneed PK, Shu HKG, *et al*. Radiosurgery for brain metastases: relationship of dose and pattern of enhancement to local control. *Int J Radiat Oncol Biol*

Phys 1997; 37: 375-383.

21. Pirzkall A, Debus J, Lohr F, *et al*. Radiosurgery alone or in combination with whole-brain radiotherapy for brain metastases. *J Clin Oncol* 1998; 16: 3563-3569.

Figure legends

.

Figure 1: A case of brain metastasis near the primary visual cortex (case 2). A) An enhanced MRI with dipoles for the primary visual cortex is shown. The left primary visual cortex is normally located, whereas the right primary visual cortex is dislocated due to metastasis. B) PTV (black solid line), primary visual cortex (black dotted line), and isodose lines (white lines, 90%, 80%, 50% and 30% from the inside out) are shown.

Figure 2: A case of AVM close to Wernicke's area (case 17). A) T1-weighted MRI with dipoles of MEG. B) PTV (black solid line), Wernicke's area (black dotted line) and isodose lines (white lines, 90%, 80%, 50% and 30% from the inside out) are shown.

Figure 3: A case of AVM close to the corticospinal tract (case 16). A) MR-axonography; the right corticospinal tract is dislocated due to large AVM. B) PTV (black solid line), corticospinal tract (black dotted line) and isodose lines (white lines, 90%, 80%, 50% and 30% from the inside out) are shown.

Figure 4: The volume of the functional area receiving 10 Gy or more (V_{10}) or 15 Gy or more (V_{15}), and the amount of the planning target volume receiving 80% or more of the prescribed dose (V_{80}-PTV) before and after modification in the 15 sets of plans that were changed after seeing the functional information

Figure 5: MR-axonography at the event of radiation necrosis (case 4). A) Enhanced T1-weighted MRI. B) axial view of MR-axonography. C) coronal view of MR-axonography: the necrotic area (white arrow) is involved in the right corticospinal tract, which was far from the dipole of the MEG image, and which was consistent with the motor cortex (arrowhead).

Figure 1, Aoyama et al.

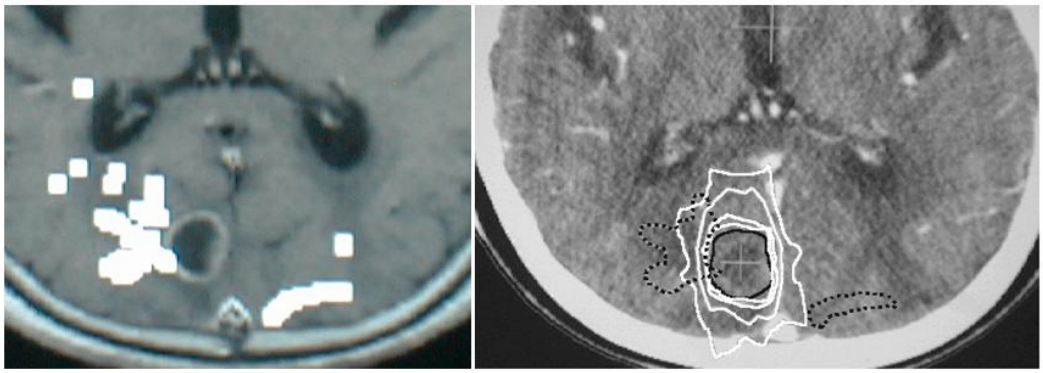

A B

Figure 2, Aoyama et al.

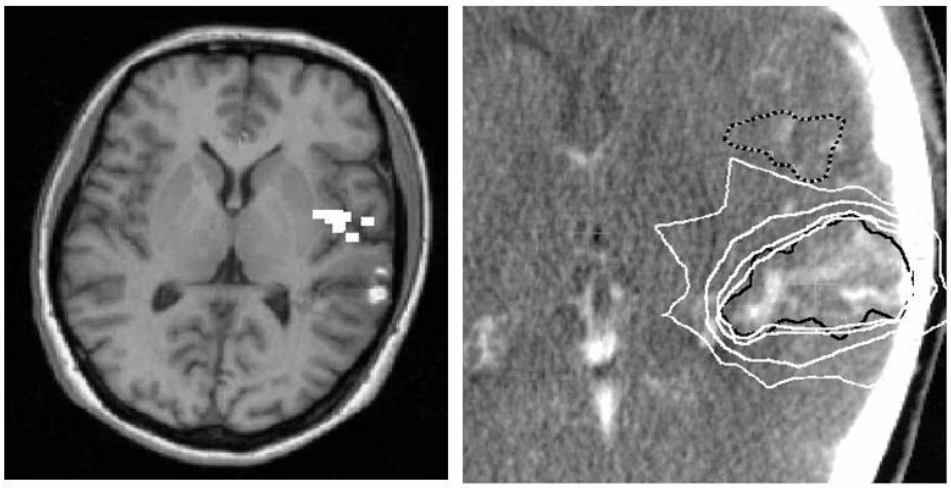

A B

Figure 3, Aoyama et al. al.

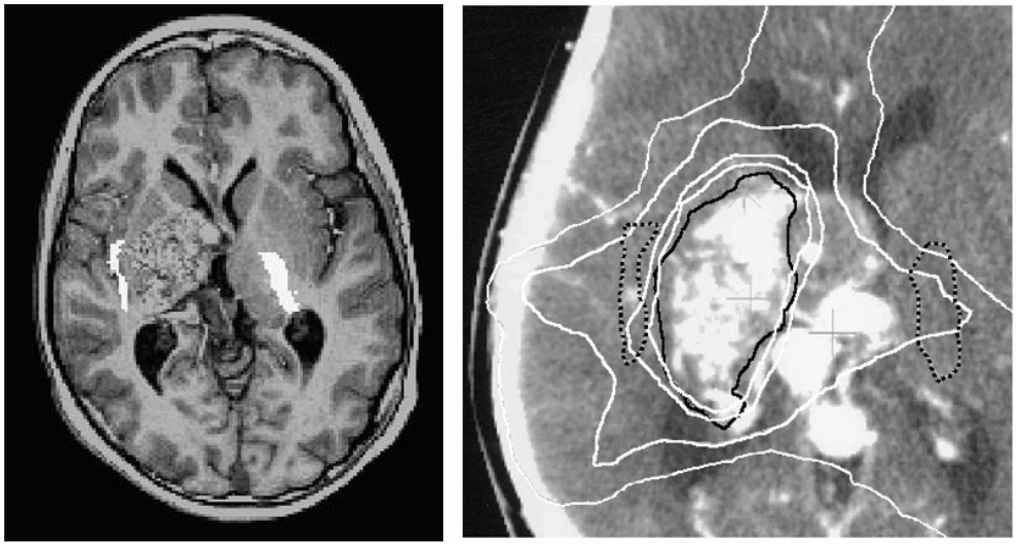

A B

Figure 4, Aoyama et al.

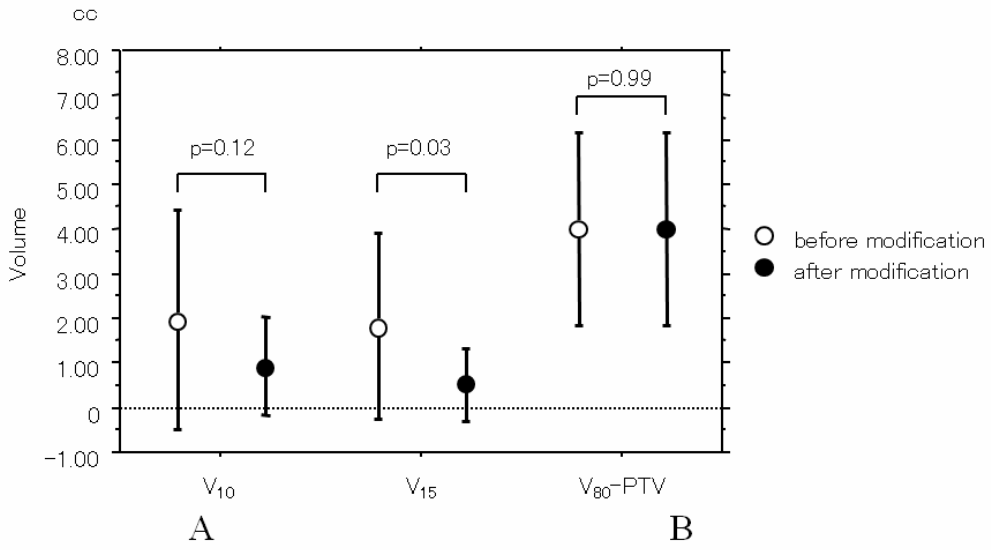

Figure 5. Aoyama et al.

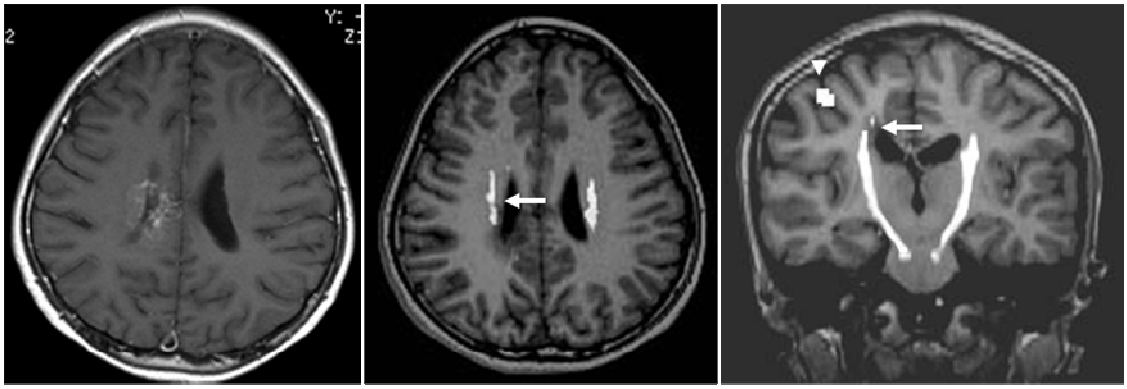

A B C

Table 1. Characteristics and results of all cases

case	disease	age	follow-up (months)	modality	identified functional area	radiation (dose/fraction)	Dmax (Gy) [d] functional information		V10 (cc) functional information		V15 (cc) functional information	
							yes	no	yes	no	yes	no
Case 1	Met	59	29	MEG [a]	Motor cortex	35Gy/4fr	16.3	18.7	0.9	6.2	0.2	5.3
Case 2	Met	82	4	MEG	Visual cortex	35Gy/4fr	18.7	19.2	1.7	3.7	0.9	5.5
Case 3	Met	75	5	MEG	Motor cortex	35Gy/4fr	18.5	19.1	2.46	3.72	1.02	3.48
	Met			MEG	Visual cortex	35Gy/4fr	11.1	18.5	0.09	0.97	0	0.89
Case 4	AVM	11	31	MEG	Motor cortex	22.5Gy/1fr	7.0	11.3	0	0.34	0	0
Case 5	AVM	41	23	MEG	Motor cortex	20Gy/1fr	16.0	16	0.32	0.32	0.16	0.16
Case 6	AVM	26	37	MEG	Motor cortex	35Gy/4fr	17.4	20.3	2.68	7.68	0.7	3.96
Case 7	AVM	45	31	MEG	Motor cortex	35Gy/4fr	7.5	9.6	0	0.11	0	0
Case 8	AVM	40	34	MEG	Motor cortex	25Gy/1fr	9.9	10.1	0	0	0	0
Case 9	AVM	21	27	MEG	Visual cortex	20Gy/4fr	6.1	9	0.11	0.11	0	0
Case 10	AVM	29	21	MEG	Wernicke's area	25Gy/1fr	3.7	3.7	0	0	0	0
Case 11	Met	64	8	MEG	Motor cortex	25Gy/1fr	25.0	26	3.06	4.5	1.98	3.5
Case 12	Met	64	20	MEG	Motor cortex	35Gy/4fr	16.1	16.1	0.76	0.76	0	0
Case 13	AVM	45	18	MEG+AX [b]	Motor cortex and CST [c]	35Gy/4fr	12.4	13.8	1.69	1.88	2.6	3.1
Case 14	AVM	60	3	MEG+AX	Motor cortex and CST	35Gy/4fr	8.0	11.7	1.09	1.59	1.4	0.5
Case 15	AVM	27	13	MEG	Visual cortex	20Gy/1fr	2.0	2	0	0	0	0
Case 16	AVM	12	9	MEG+AX	Motor cortex and CST	15Gy/1fr	15.9	15.9	4.68	4.68	0.36	0.36
Case 17	AVM	44	8	MEG	Wernicke's area	35Gy/4fr	7.3	9.7	0	0	0	0
Case 18	AVM	51	6	MEG+AX	Motor cortex and CST	35Gy/4fr	0.0	0	0	0	0	0
Case 19	AVM	65	6	MEG+AX	Motor cortex and CST	33Gy/4fr	14.8	17.2	0	0	0	0
Case 20	AVM	58	6	MEG+AX	Motor cortex and CST	35Gy/4fr	17.4	18.3	0.35	0.49	0.07	0.14

a; magnetoencephalography, b; MR-axonography, c; corticospinal tract

d. maxumum dose within functional areas converted into single fraction schdule by linear quadratic model